Chapter 6: A Low-cost approach to develop Silica doped Tricalcium Phosphate (TCP) scaffold by valorizing animal bone waste and rice husk for tissue engineering applications

6.1.Introduction

It has been estimated that more than 16-20 Million Metric Ton/Year of animal waste bone (AWB) is produced worldwide from slaughterhouses, restaurants, and household waste [1]. The disposal management of waste bone is a serious issue because these biological wastes tend to spread infectious disease through foul smell, when they are disposed directly to the ground. Also, the disposal of these wastes on agricultural and fertile land causes soil pollution resulting in infertility of land [2]. Food waste produced from restaurants and the slaughter industry causes loss in revenue as they require additional capital and resources for their disposal. The disposal of this bone waste and its management creates a hindrance to environmental protection and sustainable development [3]. If these by-products are utilized efficiently it will directly impact the economy of the country.

In order to add extra wealth from these wastes, a large number of research studies are being carried out in the field of valorization of animal wastes. Many researchers have reported the use of animal waste in different fields, like as a source of heterogeneous catalyst for the transesterification of biodiesel. AWB generally contains HAp, which can be easily converted into Tricalcium phosphate (TCP) using simple steps [4]. HAp is commonly known for its catalytic activity, thermal and chemical stability [5] and therefore it can be utilized for the production of biodiesel [5-11]. HAp derived from the waste bone of different animal possesses different elemental compositions. For example, HAp derived from bovine bone contains 52.25 wt% of CaO and 38.37 wt% of P_2O_5; whereas HAp derived from Pig bone has different elemental compositions [12-14]. Therefore, due to varying elemental composition waste bone of different animals possesses different catalytic properties [5]. Khan et al. used

Ostrich waste bone (OBW) for the development of catalyst for the production of low-cost biodiesel [5]. Chingakham et al. [6] calcined AWB followed by hydrothermal reaction to develop a heterogeneous catalyst for transesterification of biodiesel. Similarly, Jung et.al produced biodiesel by thermally induced transesterification of fish waste [7]. Prabu et al. synthesized magnetic absorbent by chemical treating and carbonizing lamb bone at 600°C for the removal of Chromium (VI) heavy metal from an aqueous solution [15]. Amiri et. al used Ostrich waste bone with hydrogen peroxide (HP) for the removal of Cobalt from waste water and to activate peroxymonosulpfate for the degradation of dye [16]. AWB has been used to prepare animal feed products as they are rich source of essential amino acid, minerals, and vitamin B_{12} [17]. Gendy et al. synthesized novel green nano bio-catalyst fluorapatite from the waste bone for the purification of wastewater released from the petroleum industry [18].

In addition to the above-mentioned applications various research studies are being carried out related to use of animal bones for the development of biological grade HAp [19, 20]. This synthesis involves simple thermal treatment of the thoroughly washed bones of animals at elevated temperatures ranging from 400 to 1200°C [21, 22]. Sintering time and temperature are the main parameters which are considered during HAp processing. Pal et al. [23] synthesized biological grade HAp from Lates calcarifer fish bone by simply heat-treating the fish bone at a different temperature ranging from 200°C to 1200°C. The developed HAp is widely used for different applications like tissue engineering, biosensors, drug carriers, etc [24].

Due to the physical and chemical properties like low crystallinity and highly substituted carbonate ions, biological HAp have higher tendency to absorb heavy metals [25, 26]. Sekine et al. [27] synthesized carbonated nano-hydroxyapatite absorbent from frozen pig

bone to capture radioisotope Strontium (^{90}Sr) for the removal of environmental pollutants. Fishbone skeleton and polymeric sponge was used by Naga et. al to develop highly porous 3D biogenic HAp scaffold with porosity 85±0.4% and compressive strength in the range of 0.13 to 1.72 MPa [28]. Porous HAp scaffold with 65% porosity has been synthesized using cortical bones of pigs as raw material and ammonium bicarbonate as a space holder material, suitable for biomedical application [29]. Deb et al. [20] utilised fish scale to develop bone scaffold with 75% porosity and compressive strength of 7.26 MPa.

With respect to the above discussion, it can be concluded that HAp/TCP derived from thermal treatment of animal bones possess excellent biocompatibility, bioactivity, and osteoconduction properties. The porous scaffold synthesized using these HAp exhibits excellent biological fixation with the host tissue at the implantation site [30-34]. In spite of the above-mentioned advantages, it has been found that due to lack of mechanical strength, these scaffold experiences fast revascularization. Thus, their trabeculae are more easily absorbed and hence their pore structure becomes weaker and fails in load-bearing applications [35, 36]. The compressive strength of bio-scaffold in the range of 1-10 MPa is ideally suitable for tissue engineering applications [37]. Therefore, it is important to develop mechanically stable HAp based scaffolds mimicking the properties of natural bone. Different approaches have been adopted to increase bioactivity and strength of HAp based ceramic scaffolds. Among which the addition of Silica and bioactive glass to the HAp matrix is of common practice [38, 39]. Bioactive glass of type Na_2O-CaO-SiO_2 supports the phenomenon of osteointegration because they produce Silanol (Si-OH) group in biological medium which initiates nucleation of HAp [40]. Addition of SiO_2 particles is a common approach to enhance mechanical properties of scaffolds [41]. The use of SiO_2 as a reinforcement phase is

recommended because of its biocompatibility, bioactivity, corrosion resistance, and anti-oxidant properties [42]. The most important requirement of any scaffold structure used for tissue engineering application is that each scaffold material should be biocompatible and should favor the bone cell attachment and differentiation on their surface [43].

Thus, considering the benefits of use of waste materials, in the present research work is an approach to develop silica doped TCP scaffold by utilizing HAp and SiO_2 from AWB and RH respectively. RH is used to perform multiple functions, which primarily acts as a space holder material in addition to the cheap source of silica during processing of the scaffold [41]. The physical, mechanical, and biological properties of the developed scaffold have been studied and compared with that of natural bone. The developed scaffold can be used as a natural bone substitute for tissue engineering applications. The present work creates a scope for sustainable development by valorizing animal and agricultural waste.

6.2.Experimental

6.2.1. Raw material Synthesis and Characterization

The raw materials used in the study was waste bone left out from restaurants and butcher shops, and rice husk obtained from local agricultural farms. The waste bone of bovine, goat, lamb, fish and chicken are used in the study. Waste bone was washed thoroughly so that unwanted materials like bone marrow, spices, etc can be washed away using deionized water. Washed bone was boiled along with common salt in order to degrease it for 2 hours followed by drying and crushing in the oven and grinder respectively. Similarly, RH was washed 3 times using deionized water so that impurities like clay, stone, etc can be removed. The washed RH was dried in the oven followed by crushing in a blender to convert it into RH powder. The RH powder and Bone Powder (BP) were sieved and powder of different sizes

was collected. Sucrose solution was used as a binder throughout the experiment. Thermal degradation behavior of BP, RH, and Sucrose was studied using Thermogravimetric analysis (TGA). SEM of pure BP and RH was carried out to study their surface morphology. To study the chemical changes taking place during sintering pure BP was characterized by means of FTIR.

6.2.2. Synthesis of the Porous Scaffold

BP powder (63-180 μm) and RH powder were used to prepare samples. RH powder of 63-180 μm particle size was used as a space holder material and source of silica as well. 0.04 wt% sucrose solution had been used as a binder for making green compacts. BP and RH powder of different wt% were mixed in mortar pestle along with 0.04 wt% of sucrose solution followed by dry compaction in the hydraulic press. A cylindrical die of 16 mm diameter was used to fabricate green compacts. To represent samples of different compositions a general formula $^{a}BP^{b}RH$ was used where BP represents bone powder and RH stands for rice husk powder. In this formula, a, and b are variables where 'a' represents wt% of BP and 'b' represents wt% of RH powder. The prepared green compacts were sintered at an elevated temperature of 1000°C and 1300°C to get HAP-SiO_2 based porous scaffold as shown in Fig. 6.1. The schematic diagram comprised of all the manufacturing steps are shown in Fig. 6.2.

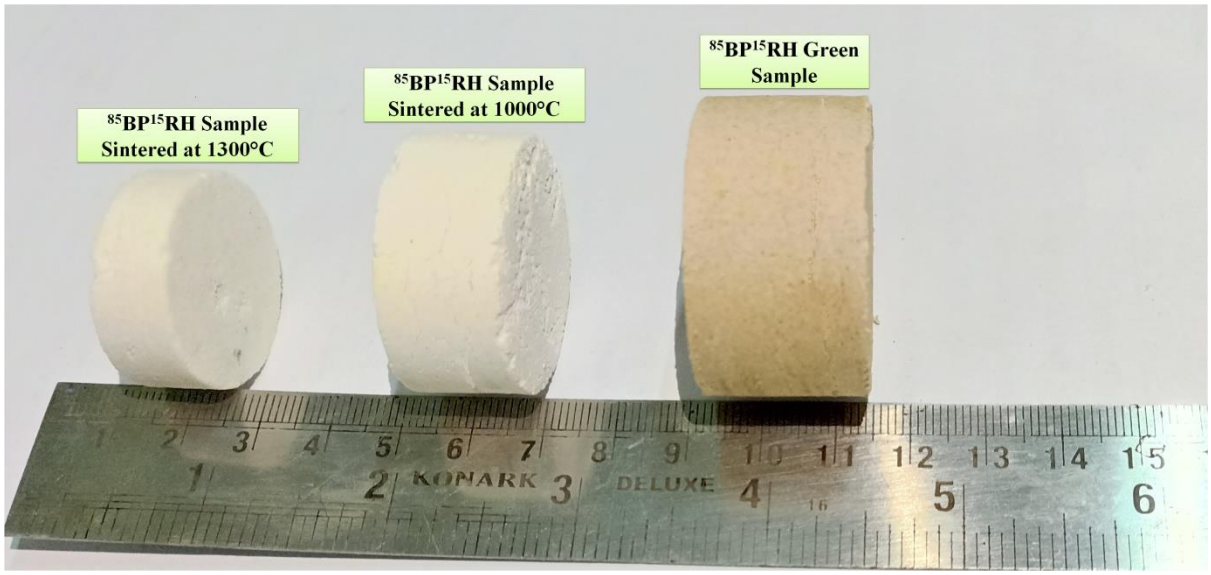

Fig. 6.1. Representative Green and sintered samples prepared using BP, RH and sucrose (as the binder). The effect of sintering temperature can be visualized by volumetric contraction and change in color of the samples.

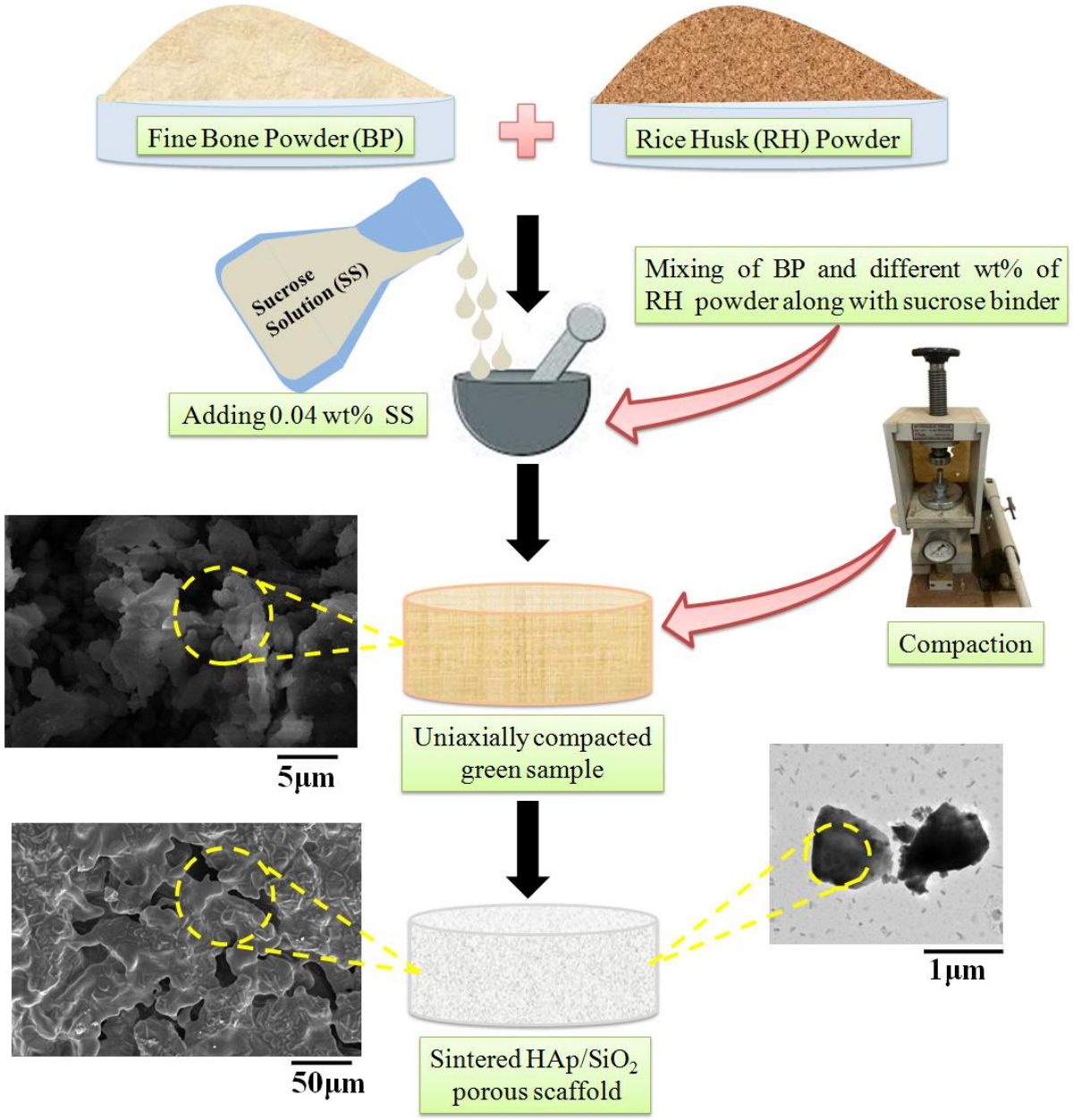

Fig. 6.2. Schematic representation for the fabrication process of HAp-SiO_2 scaffold

6.2.3. Characterization

The apparent porosity of the sintered porous samples was measured by water immersion technique based on the Archimedes principle. To identify the functional groups and phases present, the sintered samples were characterized by Fourier Transform Infrared (FTIR-

BRUKER (Yokohama, Kanagawa, Japan), TENSOR 27-3772) spectroscopy, and X-ray diffraction respectively. Surface and particle morphology of HAP-SiO_2 porous scaffold were characterized by Scanning Electron Microscopy (SEM, FEI Inspect S30 Sweden) and High-Resolution Transmission Electron Microscopy (HRTEM FEI, TECNAI G2-20 TWIN, Eindhoven, Netherlands) respectively. Elemental compositions of all the samples were studied by Energy Dispersive X-Ray spectroscopy (EDS).

6.2.4. Evaluation of Bioactivity

To determine the bioactivity of the HAp-SiO_2 scaffold, samples were immersed in simulated body fluid (SBF) and incubated for different periods. The SBF was prepared according to the Kokubo method [41] in 1000ml of deionized water and the samples were incubated in SBF for 7 and 14 days. After the mentioned incubation period the samples were removed from the solution and dried in the oven to remove trapped moisture content. The surface and elemental characteristics of these dried samples were studied by SEM and EDS analysis.

6.3.Results and Discussion

6.3.1. Thermal degradation behavior of BP, RH, and Sucrose

Thermal degradation behavior of BP, RH and sucrose was studied through TGA and their results are shown in Fig. 6.3. The degradation of BP takes place in three different stages initiating with the evaporation of entrapped water, followed by decomposition of organic material and finally dehydroxylation, and formation of phosphate ions. The first stage of degradation initiates between room temperature and 150°C. In the second stage, combustion of organic content i.e., collagen takes place between 200°C and 600°C. In the final stage of combustion i.e., between 600°C to 1000°C, the decomposition of structural carbonate takes place, due to release of carbon dioxide. It can be concluded that about 35% of total weight

loss was achieved and the remaining 65% was burnt-out residue, a similar observation was also reported by Olsen et.al. [42]. The above analysis indicates that all the organic content of raw bone is eliminated during heat treatment. Thermogravimetric analysis of RH and sucrose shows similar decomposition behavior, the major weight loss takes place between 200°C to 480°C which can be attributed to burnout of organic constituents and combustion of carbonaceous phases like cellulose and hemicelluloses. It can be observed from Fig. 3 that the ash content of sucrose is almost negligible and nearly 15% of ash was obtained after combustion of RH [43].

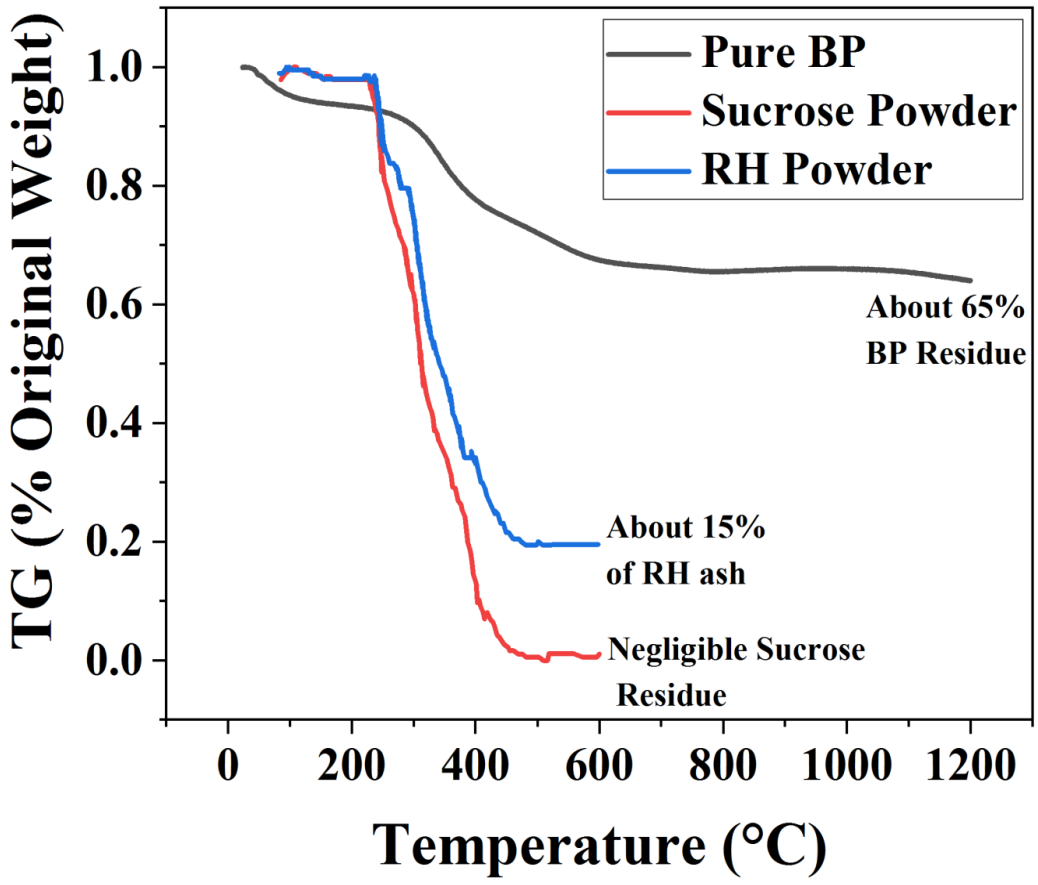

Fig. 6.3. Thermogravimetric analysis (TGA) of BP, RH and Sucrose in air

6.3.2. Phase analysis of porous HAp-SiO_2 composite

Fig. 6.4 shows the XRD diffraction pattern of the composites sintered at different temperatures with two hours of holding time. The effect of addition of RH and sintering temperature on transformational behaviour of HAp to TCP was studied. Sample $^{100}BP^{0}RH$ sintered at 1000°C shows sharp peak of HAp when compared with standard JCPDS card whereas sample $^{85}BP^{15}RH$ sintered at 1000°C shows the additional peak of TCP indicating the initiation of phase transformation of HAp to TCP due to the presence of SiO_2 (by-product of burnt RH). Some peaks of SiO_2 are also observed in XRD pattern which may be due to unreacted SiO_2. XRD analysis of $^{100}BP^{0}RH$ and $^{85}BP^{15}RH$ sintered at 1300°C shows increase in the intensity and sharpness of TCP peaks which is due to combine effect of temperature and SiO_2 in HAp to TCP phase transformation. Semi-quantative phase analysis of the samples sintered at different temperatures i.e. 1000°C, 1100°C, 1200°C, and 1300°C are studied with the help of X'Pert High Score software and the percentage of HAp, TCP and SiO_2 phases formed are shown in Table 6.1. From Table 6.1 it is evident that as the sintering temperature and weight percent of RH increases the transformation of HAp to TCP increases. It was found that sample $^{85}BP^{15}RH$ sintered at 1300°C consists of 67% of TCP phase and 10% of HAp phase confirming the role of silica and sintering temperature in phase transformation of HAp to TCP. A detailed discussion on the mechanism of HAp to TCP transformation is presented in the next section of this article.

Table 6.1 Semi- quantitative analysis of phases formed in silica doped TCP scaffold sintered at different temperatures

Sample Code	Sintering Temp.	HAp%	TCP%	SiO_2%
$^{100}BP^{0}RH$	1000 °C	100	0	0
$^{85}BP^{15}RH$	1000 °C	80	11	9

$^{100}BP^{0}RH$	1100°C	90	10	0
$^{85}BP^{15}RH$	1100°C	75	15	10
$^{100}BP^{0}RH$	1200°C	86	14	0
$^{85}BP^{15}RH$	1200°C	65	25	10
$^{100}BP^{0}RH$	1300°C	54	46	0
$^{85}BP^{15}RH$	1300°C	11	76	13

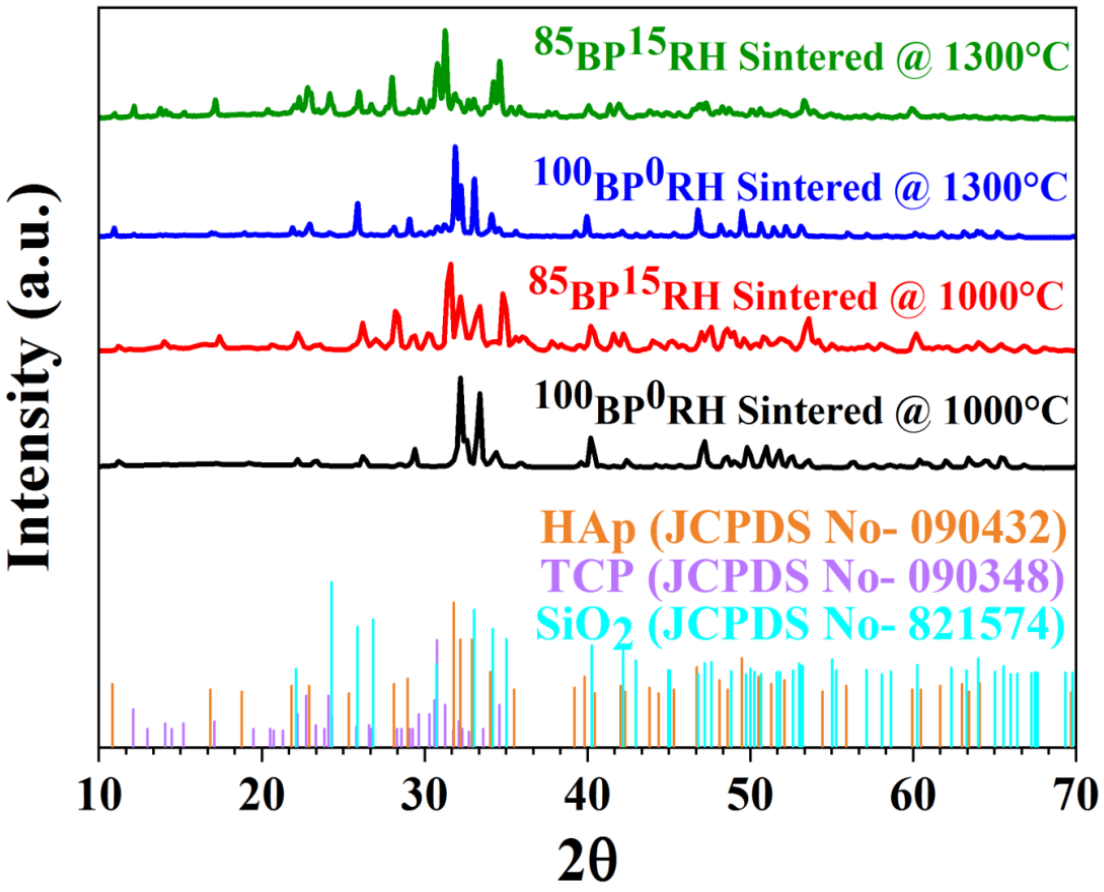

Fig. 6.4. XRD diffraction pattern of BP samples sintered at different temperatures with different wt% of RH

6.3.3. Mechanism of Transformation of HAp to TCP

The transformation of HAp to TCP is generally based on two parameters i.e., the effect of sintering temperature and the amount of silica added in the HAp matrix. The transformation mechanisms based on these two parameters are discussed systematically. During the high temperature sintering of HAp two different phenomenon's i.e., decomposition and dehydroxylation takes place [47]. During dehydroxylation OH ions loose from HAp and forms oxyhydroxyapatite. At a temperature between 800-1300°C reversible dehydroxylation takes place along with HAp decomposition. During this process HAp decomposes into TCP (α and β TCP) according to the reaction in Eq. (1). Similarly, the mechanism of SiO_2 promoting the phase transformation of HAp to TCP can be explained by the interfacial reaction between HAp and RH derived SiO_2. As explained above due to high temperature sintering a phenomenon of decomposition and dehydroxylation takes place. During dehydroxylation process OH radicals loose from the material and creates vacancies in the HAp lattice. These positively charged defects will be compensated by the substitution of Si^{4+} at P^{5+} site leading the transformation of HAp to Si-TCP. The chemical stability of the formed Si-TCP would be possible either by the formation of O^{2-} vacancies or due to the presence of excess calcium Ca^{2+}. This will compensate the charge compensation created by Si^{4+} substitution in the place of P^{5+} in the TCP lattice. The charge compensation process either by formation of O^{2-} vacancy or presence of excess Ca^{2+} is dependent on the SiO_2: HAp mole ratio. M. Sayer et al. [48] reported that charge compensation process either by formation of O^{2-} vacancies or due to the presence of excess calcium Ca^{2+} is dependent on molar ratio of SiO_2: Hap. A molar ratio of at least 0.33 of SiO_2: HAp is required for the transformation of Si-TCP having chemical composition of $Ca_3[(P_{0.9}Si_{0.1}O_{3.95})]_2$ when charge of Si-TCP is

compensated by formation of O^{2-} vacancies. And a minimum of 0.25 molar ratio of SiO_2: HAp is required for the transformation of Si-TCP having chemical composition of $Ca_{3.08}[(P_{0.92}Si_{0.08}O_4)]_2$ when charge of Si-TCP is compensated by incorporation of excess calcium Ca^{2+}. It can be concluded that the overall phase transformation initiates with the loss of OH radical during Si addition and Si-TCP phase can be formed. The extent of phase transformation depends on the SiO_2: HAp mole ratio which can be varied from 0.25-0.33 depending on the method of charge compensation weather oxygen vacancies or excess calcium. Apart from formation of Si-TCP, SiO_2 also promotes formation of a glassy phase when SiO_2: HAp mole ratio exceeds to 1. The schematic diagram of the explained mechanism is shown in Fig. 6.5. The above discussion was also supported by previous studies which reports formation of unique Si-TCP crystalline phase while sintering HAp in the presence of SiO_2 at higher temperature [48, 49]. It is important to mention that during high-temperature processing certain by-products like CaO and P_2O_5 are formed according to the reaction in Eq. (1) and (2). These by-products further combine with SiO_2 to form a bioactive glassy network of Ca-Si-P-O phase [48, 50]. Thus, from the above analysis it can be concluded that due to high temperature sintering and addition of SiO_2 in HAp matrix a phenomenon of decomposition and dehydroxylation takes place resulting in transformation of HAp to TCP. The addition of SiO_2 during higher temperature sintering enhances HAp to TCP transformation along with the formation of bioactive glassy component and as the mole ratio of HAp: SiO_2 increases this transformation increases.

$$Ca_{10}(PO_4)_6(OH)_2 \longrightarrow 3Ca_3(PO_4)_2 + CaO + H_2O \qquad (1)$$

$$10Ca_3(PO_4)_2 + 2SiO_2 \longrightarrow 10Ca_3(P_{0.9}Si_{0.1}O_{3.95})_2 + P_2O_5 \qquad (2)$$

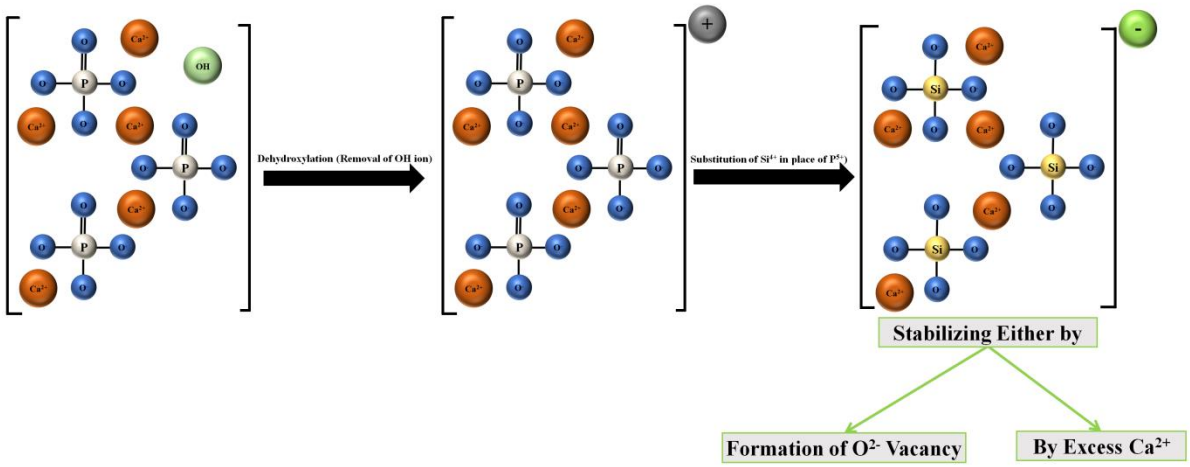

Fig. 6.5. Mechanism of phase transformation of HAp to TCP by Si substitution

6.3.4. FTIR analysis

The effect of sintering on raw and sintered samples can be distinguished through visual observation. As the sintering temperature increases from 900°C to 1400°C the color of the samples changes from yellowish to off-white followed by complete white color. The reason behind this change in color can be attributed to the decomposition of organic phases like protein and collagen present in raw bone [51, 52]. The vibrational spectra shown in Fig. 6.6 (a) also confirms the above discussion. The FTIR band present at 1640cm^{-1} corresponds to Amide I of collagen [53] which was present in raw bone, and as the sintering temperature increases, this collagen disappears completely, Fig. 6.6 (b, c). Further, the FTIR spectra demonstrate the presence of different functional groups like phosphate (PO_4^{3-}), carbonate (CO_3^{2-}), and hydroxyl (OH^-) groups in the samples. The broadband appeared at 961.5 cm^{-1}, 1015 cm^{-1}, and 1087 cm^{-1} corresponds to phosphate groups [54, 55]. The band that appeared at 1453-1470 cm^{-1} correlates with the presence of characteristics peaks of CO_3^{2-} [56]. Thus, the presence of sharp peaks of (PO_4^{3-}) and (OH^-) confirms the formation of HA and TCP

[57]. The vibrational spectra of samples mixed with different 15 wt% of RH and sintered at 1000°C and 1300°C reveals the presence of absorption bands of SiO_2 Fig. 6.6 (d, e). The absorbance band around 1130-1000 cm^{-1} corresponds to the siloxane group (Si-O-Si) and the absorption band around 1625 cm^{-1} and 3400-3200 cm^{-1} corresponds to the presence of silanol group (Si-OH). It is important to mention that HAp and SiO_2 share several similar vibrational modes which may be due to similarities in vibrational characteristics between SiO_4^{4-} and PO_4^{3-} [58].

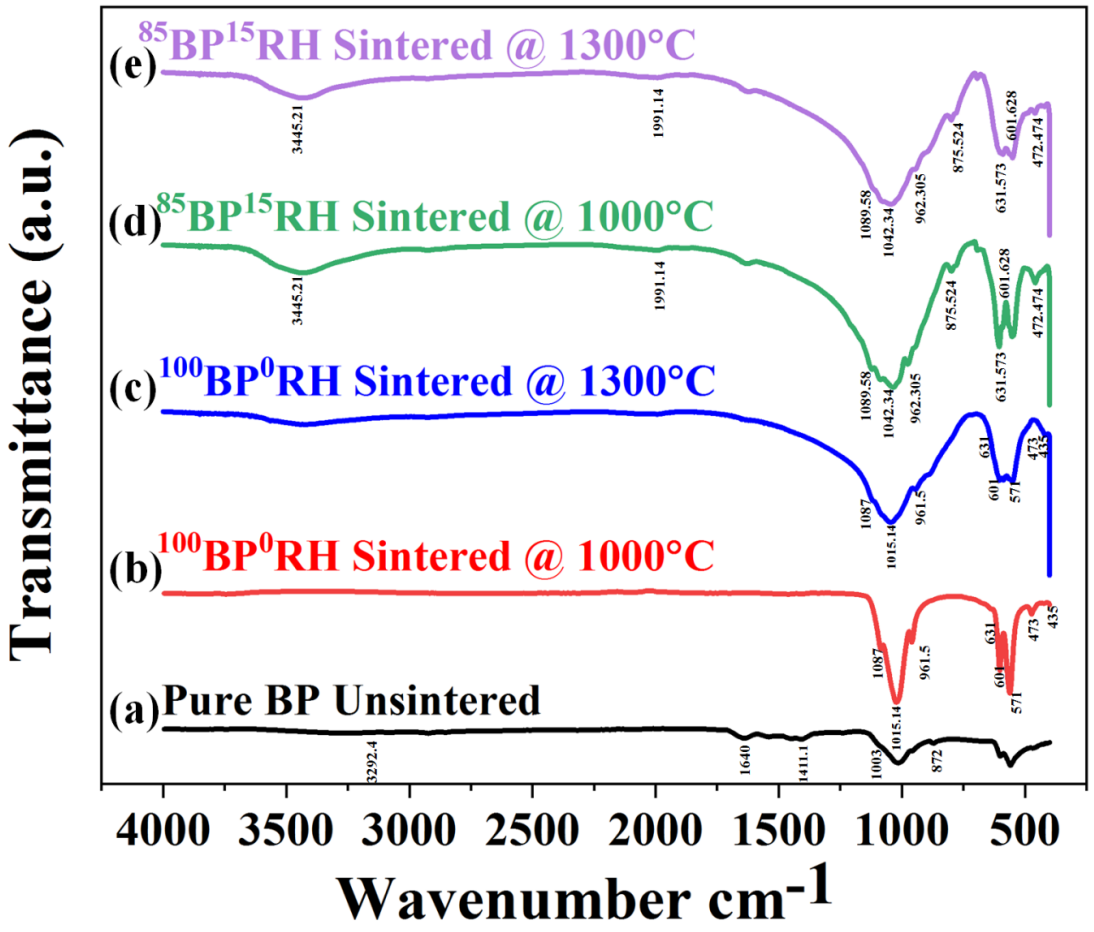

Fig. 6.6. FTIR analysis of (a) unsintered pure BP, (b, c) pure BP samples sintered at 1000°C and 1300°C, (d, e) samples sintered at 1000°C and 1300°C with 15 wt% of RH

6.3.5. Morphological analysis of scaffold by SEM and TEM imaging

Scanning electron micrographs of raw BP and RH powder are shown in Fig.6.7. The raw BP particles appear to be agglomerated and RH particles appear to be micro rod-shaped fibers as shown in the SEM micrograph. SEM images of the samples shown in Fig. 6.8 (a-d) reveal the microstructural change in the HAp matrix due to the addition of SiO_2 and high-temperature sintering. Fig.6. 8 (a) and (b) show pure HAp samples sintered at 1000°C and 1300°C respectively. The initiation of grain growth of TCP crystals can be easily visualized from Fig. 6.8 (a) and as the sintering temperature increases the phenomenon of grain growth takes place. The fully developed grains with clear demarcation in grains and grain boundary were observed at higher sintering temperatures. Fig 6.8 (c) and (d) show SEM micrographs of BP samples with 15 wt% of RH powder sintered at 1000°C and 1300°C respectively. Due to the incorporation of SiO_2 in the HAp matrix and high-temperature sintering, a glassy phase network was observed across the HAp and TCP crystals. Due to the excess amount of glassy phase, it was difficult to differentiate the grain boundary, which was easily visible earlier in Fig. 6.8 (b). The presence of pores on the samples seen in the micrographs, are the result of the carbonization of randomly distributed RH powder. Thus, from the microstructural study, it can be concluded that the addition of RH performs multiple roles. Initially, it acts as a pore former and formerly the burnt-out residue of RH acts as a source of SiO_2 which plays a major role in the formation of crystalline-glassy composite. The TEM micrograph of the samples sintered at 1300°C shows irregular drop-like HAp/TCP crystals as shown Fig. 6.9 (a, b). TEM micrographs of samples at higher magnification show the formation of hexagonal HAp and TCP structure as confirmed by their characteristic lattice spacing of 0.526 nm and 0.38 nm respectively. Elemental analysis of the samples was recorded by EDS as shown in Fig.

6.9 (c). The Ca/P molar ratio of all the samples sintered at 1000°C and 1300°C was in the range of 1.95-1.99 and 2.35-2.9 respectively. These results are similar to the theoretical value of the Ca/P molar ratio of HAp (1.67) and TCP (1.5) [59].

The elemental analysis obtained from EDS and XRF reveals varying amount of CaO, P_2O_5, and Ca/P ratios under different sintering conditions (Table 2). The Ca/P ratio of all the samples was in the range of 1.93 to 2.7 which was higher than that of the stoichiometric value of pure HAp (1.67) and TCP (1.5). This deviation in the Ca/P ratio can be attributed to the presence of other calcium phosphate phases in the HAp lattice. The higher value of Ca/P ratio was due to the higher substitution of carbonate ions at the phosphate site [60].

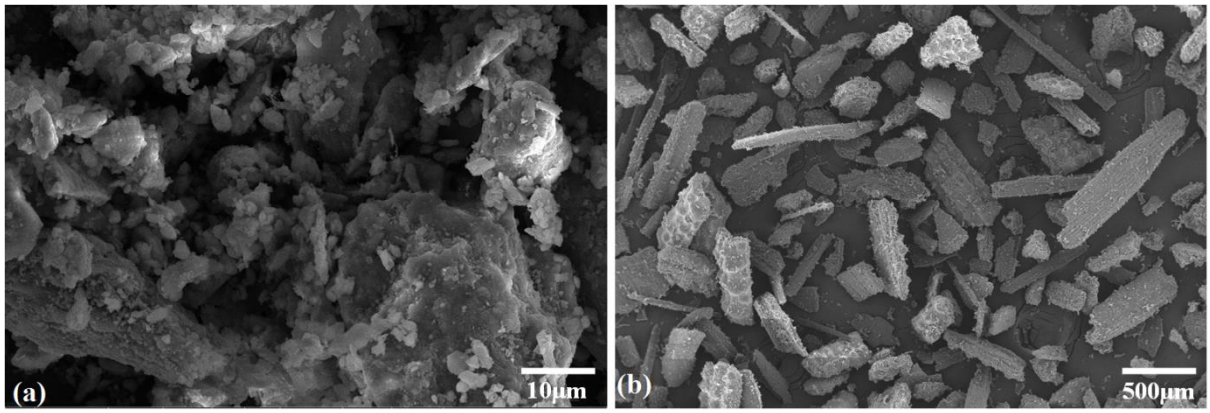

Fig. 6.7. SEM of thoroughly washed (a) raw BP and (b) dried RH powder

Table 6.2 Elemental composition, Ca/P ratio, and physical properties of unsintered and sintered samples.

Sample	**Colour**	**Change in Volume (%)**	**CaO[a] (wt %)**	**P_2O_5[a] (wt %)**	**Ca/P[b] ratio**
Pure BP Unsintered	Light Yellow	0*	56.33	37.32	2.705
BP Sintered @ 1000°C	Off White	15	59.85	35.06	1.93
BP Sintered @ 1300°C	White	23	-	-	2.33

* Average initial volume of cylindrical pellets before heat treatment is considered as 100%.

a Data obtained from XRF analysis

b Data obtained from EDS

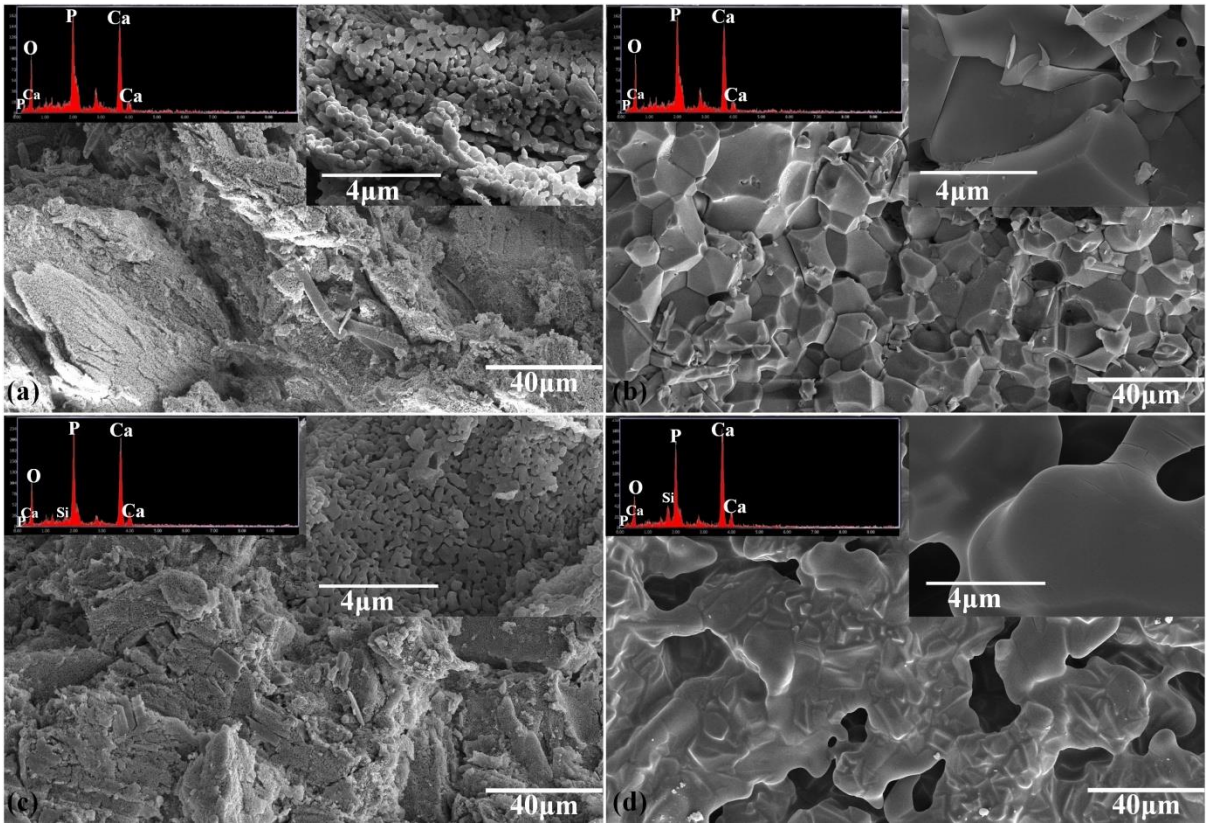

Fig. 6.8. SEM and EDS analysis of (a) $^{100}BP^{0}RH$ sintered at 1000°C, (b) $^{100}BP^{0}RH$ sintered at 1300°C, (c) $^{85}BP^{15}RH$ sintered at 1000°C, (d) $^{85}BP^{15}RH$ sintered at 1300°C at different magnifications

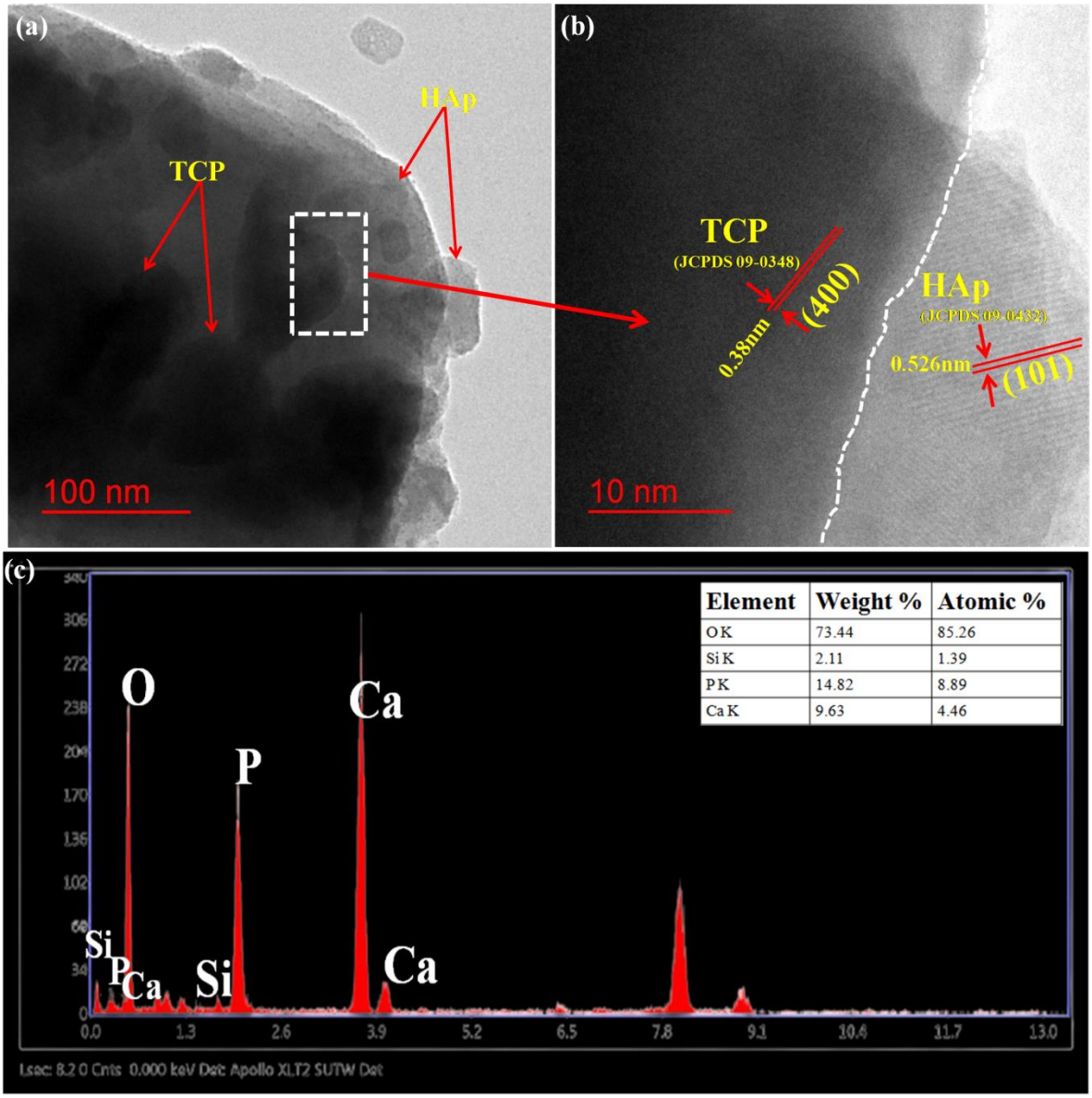

Fig. 6.9. (a) TEM, (b) HRTEM and (c) EDS analysis of ^{85}BP^{15}RH sintered at 1300°C

6.3.6. Porosity and Mechanical properties

Figure 6.10 (a, b) shows the effect of RH content on the porosity and compressive strength of the scaffold sintered at different temperatures i.e., 900°C to 1400°C respectively. It is observed that for the samples sintered in the range of 900°C to 1100°C, the effect of RH content on open porosity is directly related. The open porosity increases from 54-61% with the increase of RH wt% from 5-20 wt%. However, an inverse relation is detected for the

samples sintered in between 1200°C to 1400°C. The open porosity value decreases up to 34% for the same wt% of RH when sintered above 1200°C. This is due to the phenomenon of the formation of the Ca-Si-P-O glassy phase which has been discussed earlier. Figure 6.11 shows the statistical analysis of the pores formed throughout the composites sintered at different temperatures. SEM images were analyzed with the help of ImageJ software to measure the average diameter of the pores. Pure BP samples sintered at 1000°C and 1300°C have average pore size of 0.328 and 8.19 µm respectively. However number of pores decreases with the increase in temperature making scaffold overall less porous. Similarly samples added with 15% RH and sintered at 1000°C and 1300°C shows average pore size of 2.828 and 15.97 µm respectively. The compressive strength of the samples was in the range of 0.78 to 4.1 MPa. The compressive data are in line with the open porosity results. The obtained physical and mechanical properties of the developed scaffolds are analyzed and compared with that of natural human bones and previously reported work (as shown in Table 6.3) and concluded that the developed porous composite has the potential to be used for tissue engineering application.

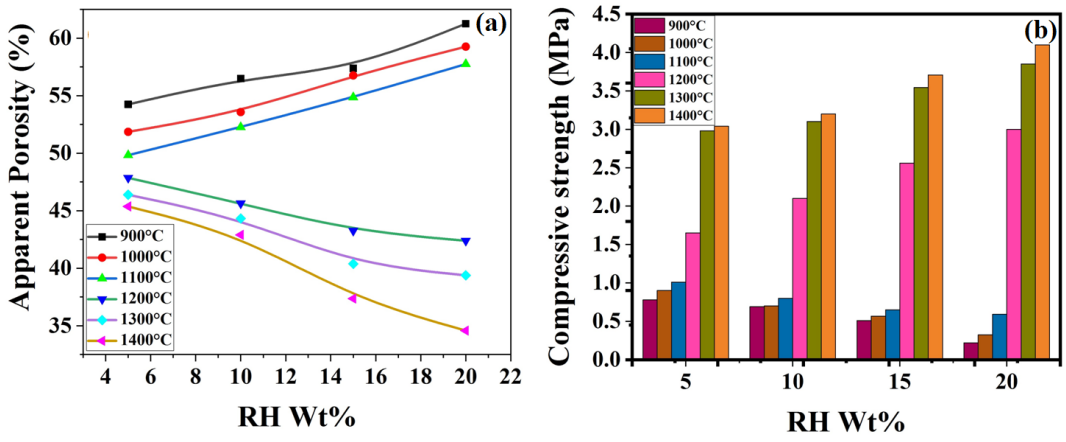

Fig. 6.10. Effect of sintering temperature and RH content on the (a) apparent porosity and (b) compressive strength of the silica doped TCP scaffold

Waste Material	**Method/ Space Holder (SH) Material**	**Binder/ Solvent**	**Sintering Condition**	**Porosity (%)**	**Compressive Strength (MPa)**	**References**
Bovine Bone	Commercial Sugar	NA	900°C	76.7±0.6	1.3±0.09	[61]
Fish Bone	High-density polyethylene sponge	PVA	Initial Sintering at 600°C Final Sintering 1200°C	85±0.4	0.13±0.007 MPa	[28]
Fish Scale	Sponge Replication	Starch	1000-1400°C, 2hr	35	0.8GPa=800MPa	[62]
Pig Bone Waste	Ammonium Bicarbonate	NA	600-1000°C	65	NA	[29]
Fish Scale	solvent casting particulate leaching technique/ NaCl (SH)	Ethanol (as solvent)	1200°C, 3 hr	75±0.8	7.26±0.45	[20]
Bovine Bone	3D Printing	Glycerine (solvent)	900°C	NA	3.22±0.13 to 5.71±0.43	[63]
General Bone Waste	Rice Husk	Sucrose Solution	1000-1400°C, 2 hr	34-61	0.22 - 4.1	Present Work

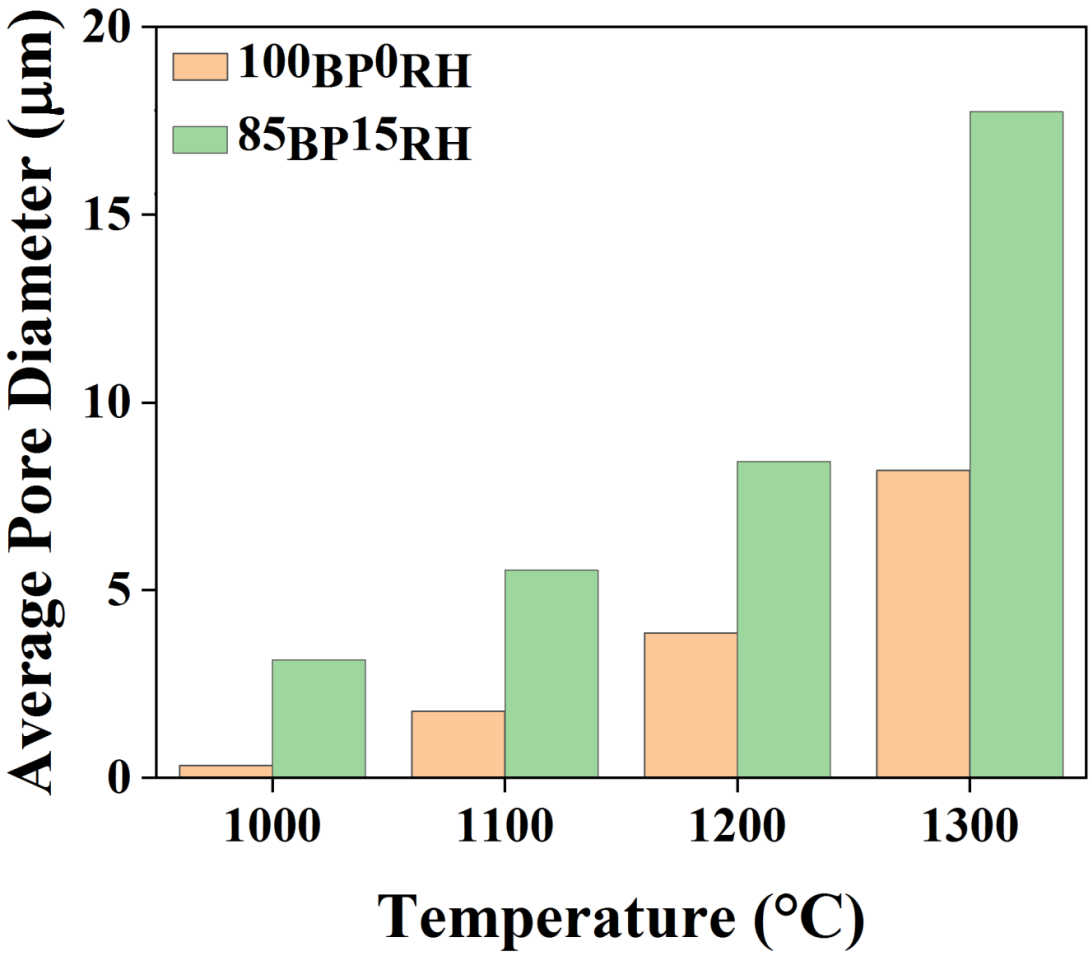

Fig. 6.11. Effect of RH content and sintering temperature on pore size of silica doped TCP scaffold

Table 6.3 Property Comparison of developed silica doped TCP scaffold with previously reported work

6.3.7. Evaluation of Bioactivity

SEM images of porous scaffold immersed in SBF for 7 and 14 days show in-vitro bioactivity i.e., ability of the scaffold to form a bone-like apatite layer on its surface when introduced in a biological environment. It can be visualized from SEM images that as the wt% of RH increases from 5% to 20%, the ability of the samples to form an apatite layer on their surfaces increases. It is evident from the images that this apatite layer is covering the HAp-SiO_2 surface uniformly. Under higher magnification, these layers appear like a continuous array of petals-like structures spread over the surface of HAp-SiO_2 scaffold, as shown in Fig. 6.12 (d). This phenomenon can be easily understood by the fact that the formation of an apatite layer on the artificial body is supported by the presence of Silanol (Si-OH) functional group, the only site where nucleation of apatite crystal initiates. As soon as the apatite nuclei forms, they start propagating throughout the surface by consuming Ca^{2+} and P^{5+} ions from the surrounding biological environment i.e., SBF. It is also worth mentioning that due to the addition of SiO_2 the transformation of HAp to TCP increases. TCP is well known for its biocompatibility and osteoconductivity because of its higher solubility w.r.t HAp [60]. Thus, from the above analysis, it can be concluded that the addition of silica in the HAp matrix is beneficial. It promotes HAp to TCP transformation along with the increase in apatite nucleation site by providing a silanol group. Fig. 6.12 (e) shows the EDS analysis of $^{85}BP^{15}RH$ sintered at 1300°C and immersed in SBF for 14 days. EDX spectra shows the presence of Ca and P and the Ca/P ratio of the sample was 1.43 and 2.53 for 7 and 14 days of immersion respectively. It can be suggested that the P ions were released immensely on day 7 and formed apatite layer on day 14, as the Ca/P ratio was close to bone like apatite.

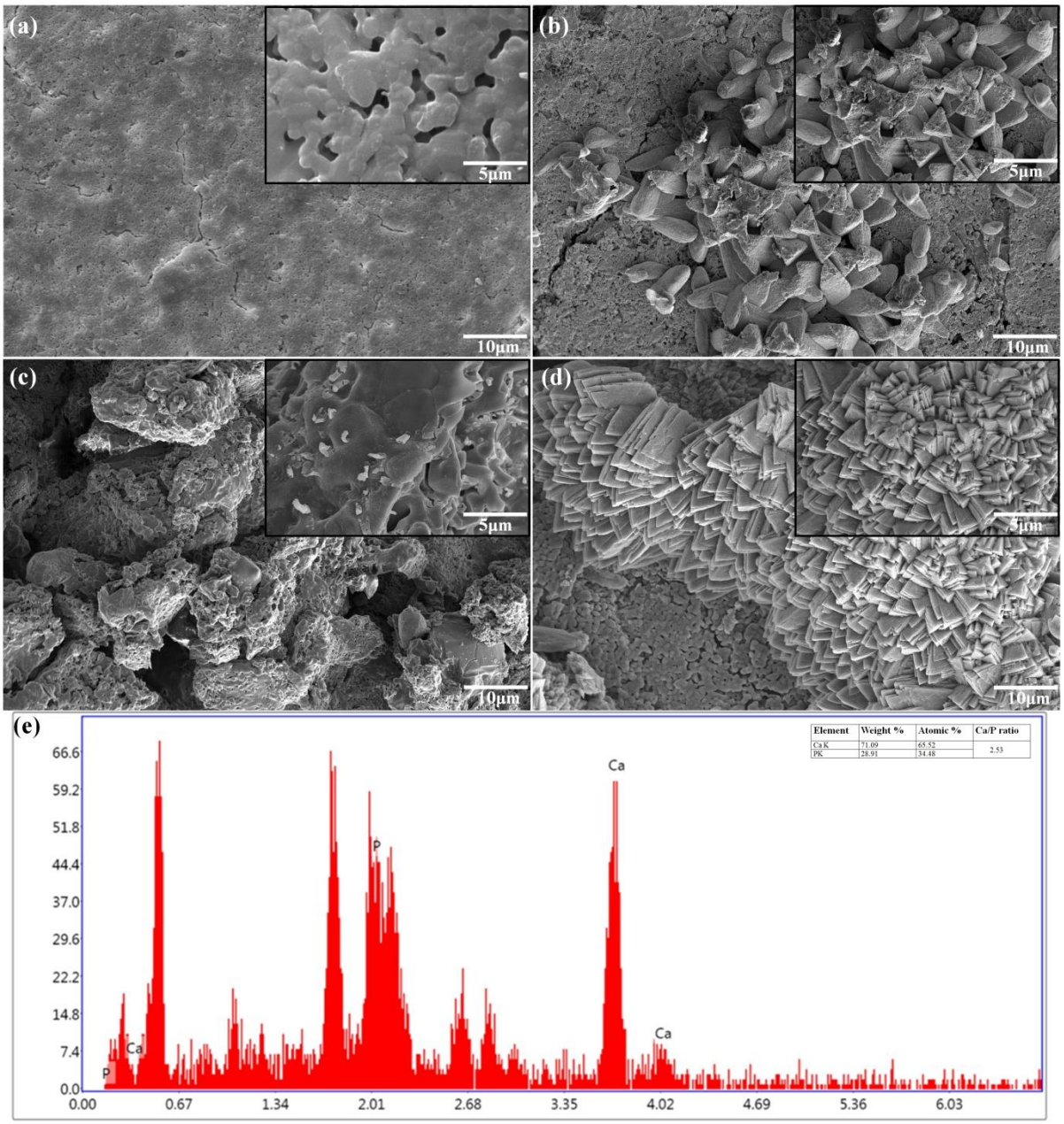

Fig. 6.12. SEM micrographs of (a) $^{100}BP^{0}RH$, (b) $^{85}BP^{15}RH$ sintered at 1300°C and immersed in SBF for 7 days, and (c) $^{100}BP^{0}RH$, (d) $^{85}BP^{15}RH$ sintered at 1300°C and immersed in SBF for 14 days, (e) EDS analysis of $^{85}BP^{15}RH$ sintered at 1300°C and immersed in SBF for 14 days.

6.4.Conclusion

The present research work is a low-cost novel approach to develop silica doped TCP scaffold by utilizing agricultural and animal wastes. High-temperature sintering and addition of silica (by-product burnt RH) results in the transformation of pure HAp to TCP, and as the sintering temperature and wt% of RH increases the crystallinity of the TCP phase increases. The main reason behind the phase transformation of HAP to TCP is attributed to high temperature sintering and addition of silica. Due to high temperature sintering decomposition and dehydroxylation takes place along with this an interfacial reaction between HAp and SiO_2 also takes place, which leads to phase transformation. TGA analysis of raw bone shows complete removal of organic constituents at 1200°C and about 65% of burn out residue is produced. During initial stages of firing, RH powder acted as a space holder and at later stages of sintering SiO_2 from RH acts as a reinforcement phase in the HAp matrix. The HAp combines with SiO_2 (burnt-out residue of RH) to form silica doped TCP composite at an elevated sintering temperature and enhances the compressive strength of the porous scaffold. Due to the incorporation of SiO_2, major changes are observed in the microstructural and biological properties of HAp. A bioactive glassy network of Ca-Si-P-O amorphous phase is observed across the matrix which is also responsible for the enhancement of bioactivity of the scaffold. The physical and mechanical properties of the porous scaffold are similar to that of natural bone. Thus, the above study shows the possibility of valorizing animal and agricultural waste for the development of TCP based scaffold potentially suitable for tissue engineering applications.

References

[1] Y. Liu, J. Chen, Phosphorus cycle, Encyclopedia of ecology second edition, 4 (2014) 181-191, https://doi.org/10.1016/B978-0-12-409548-9.09043-6, 978-0-444-64130-4.

[2] M. Boutinguiza, J. Pou, R. Comesana, F. Lusquinos, A. de Carlos, B. Leon, Biological hydroxyapatite obtained from fish bones, Materials Science and Engineering C 32 (2012) 478–486, http://dx.doi.org/10.1016/j.msec.2011.11.021.

[3] W. Russ, R. M. Pittroff, Utilizing waste products from the food production and processing industries, Critical Reviews in Food Science and Nutrition, 44 (2004) 57-62, https://doi.org/10.1080/10408690490263783.

[4] X. Y. Lü, Y. B. Fan, D. Gu, W. Cui, Preparation and Characterization of Natural Hydroxyapatite from Animal Hard Tissues, Key Engineering Materials, 342-343 (2007), https://doi.org/10.4028/www.scientific.net/KEM.342-343.213

[5] H. M. Khana, T. Iqbala, C. H. Alia, A. Javaida, I. I. Cheemaa, Sustainable biodiesel production from waste cooking oil utilizing waste ostrich (Struthio camelus) bones derived heterogeneous catalyst, Fuel 277 (2020) 118091, https://doi.org/10.1016/j.fuel.2020.118091.

[6] C. Chingakham, C. Tiwary, V. Sajith, Waste Animal Bone as a Novel Layered Heterogeneous Catalyst for the Transesterification of Biodiesel,Catalysis Letters 149 (2019), 1100–1110, https://doi.org/10.1007/s10562-019-02696-9.

[7] J. M. Jung, J. I. Oh, Y. K. Park, J. Leed, E. E. Kwon, Biodiesel synthesis from fish waste via thermally-induced transesterification using clay as porous material, 371 (2019) 27-32, s://doi.org/10.1016/j.jhazmat.2019.02.109.

[8] Y. H. Tan, M. O. Abdullah, J. Kansedo, N. M. Mubarak, Y. S. Chan, C. N. Hipolito, Biodiesel production from used cooking oil using green solid catalyst derived from calcined fusion waste chicken and fish bones, Renewable Energy 139 (2019) 696-706, https://doi.org/10.1016/j.renene.2019.02.110.

[9] M. AlSharifi, H. Znad, Transesterification of waste canola oil by lithium/zinc composite supported on waste chicken bone as an effective catalyst, Renewable Energy 151 (2020) 740-749, https://doi.org/10.1016/j.renene.2019.11.071.

[10] T. F. Adepoju, M. A. Ibeh, A. J. Asuquo, Elucidate three novel catalysts synthesized from animal bones for the production of biodiesel from ternary non-edible and edible oil blend: A case of Jatropha curcus, Hevea brasiliensis, and Elaeis guineensis oil, South African Journal of Chemical Engineering 36 (2021) 58–73, https://doi.org/10.1016/j.sajce.2021.01.002.

[11] A. A. Ayodeji, I. E. Blessing, F. O. Sunday, Data on calcium oxide and cow bone catalysts used for soybean biodiesel production, Data in brief 18 (2018) 512–517, https://doi.org/10.1016/j.dib.2018.03.057.

[12] K. Haberko, M. M. Bućko, J. B. Miecznik, M. Haberko, W. Mozgawa, T. Panz, A. Pyda, J. Zarębski, Natural hydroxyapatite—its behaviour during heat treatment, Journal of the European Ceramic Society, 26 (2006) 537-542, https://doi.org/10.1016/j.jeurceramsoc.2005.07.033.

[13] A. Buasri, T. Inkaew, L. Kodephun, W. Yenying, V. Loryuenyong, Natural Hydroxyapatite (NHAp) Derived from Pork Bone as a Renewable Catalyst for Biodiesel

Production via Microwave Irradiation, Key Engineering Materials, 659 (2015) 216-220, https://doi.org/10.4028/www.scientific.net/KEM.659.216.

[14] T. Jia, F. Zhou, H. Ma, Y. Zhang, A highly stable waste animal bone-based catalyst for selective nitriles production from biomass via catalytic fast pyrolysis in NH3, Journal of Analytical and Applied Pyrolysis 157 (2021) 105217, https://doi.org/10.1016/j.jaap.2021.105217.

[15] D. Prabu, P. S. Kumar, B. S. Rathi, S. Sathish, K. V. Anand, J. A.Kumar O. B. Mohammed, P. Silambarasan, Feasibility of magnetic nano adsorbent impregnated with activated carbon from animal bone waste: Application for the chromium (VI) removal, Environmental Research 203 (2022) 111813, https://doi.org/10.1016/j.envres.2021.111813.

[16] M. J. Amiri, A. Faraji, M. Azizi, B. G. Nejad, M. Arshadi, Recycling bone waste and cobalt-wastewater into a highly stable andefficient activator of peroxymonosulfate for dye and HEPES degradation, Process Safety and Environmental Protection 147 (2021) 626–641, https://doi.org/10.1016/j.psep.2020.12.039.

[17] K. Jayathilakan, K. Sultana, K. Radhakrishna, A. S. Bawa, Utilization of byproducts and waste materials from meat, poultry and fish processing industries: a review, J Food Sci Technol, 49 (2012) 278-293, DOI 10.1007/s13197-011-0290-7.

[18] N. S. El-Gendy, R. A. El- Salamony, S. A. Younis, Green synthesis of fluorapatite from waste animal bones and thephoto-catalytic degradation activity of a new ZnO/green biocatalystnano-composite for removal of chlorophenols, Journal of Water Process Engineering, 12 (2016) 8–19, dx.doi.org/10.1016/j.jwpe.2016.05.007.

[19] C. Piccirillo, R. C. Pullar, D. M. Tobaldi, P. M. L. Castro, M. M. E. Pintado, Hydroxyapatite and chloroapatite derived from sardine by-products, Ceramics International, 40 (2014) 13231-13240, http://dx.doi.org/10.1016/j.ceramint.2014.05.030.

[20] P. Deb, E. Barua, A. B. Deoghare, S. D. Lala, Development of bone scaffold using Puntius conchonius fish scale derived hydroxyapatite: Physico-mechanical and bioactivity evaluations, Ceramics International 45 (2019) 10004–10012, https://doi.org/10.1016/j.ceramint.2019.02.044.

[21] C. F. R. Gutierrez, S. M. L. Restrepo, A. D. Real, M. A. Mondragón, M. E. R. García, Effect of the temperature and sintering time on the thermal, structural, morphological, and vibrational properties of hydroxyapatite derived from pig bone, Ceramics International, 43 (2017) 7552–7559, http://dx.doi.org/10.1016/j.ceramint.2017.03.046

[22] S. Joschek, B. Nies, R. Krotz, A. Gopferich, Chemical and physicochemical characterization of porous hydroxyapatite ceramics made of natural bone, Biomaterials, 21 (2000) 1645-1658.

[23] A. Pal, S. Paul, A. R. Choudhury, V. K. Balla, M. Das, A. Sinha, Synthesis of hydroxyapatite from Lates calcarifer fish bone for biomedical applications, Materials Letters 203 (2017) 89–92, http://dx.doi.org/10.1016/j.matlet.2017.05.103.

[24] P. N. Kumta, C. Sfeir, D. H. Lee, D. Olton, D. Choi, Nanostructured calcium phosphates for biomedical applications: novel synthesis and characterization, Acta Biomaterialia. 1 (2005) 65–83, https://doi.org/10.1016/j.actbio.2004.09.008.

[25] F. Fernane, M. O. Mecherri, P. Sharrock, M. Hadioui, H. Lounich, M. Fedoriff, Sorption of cadmium and copper ions in natural and synthetic hydroxyapatite particles, Material characterization, 59 (2008) 554–559, https://doi.org/10.1016/j.matchar.2007.04.009.

[26] E. Landi, G. Celotti, G. Logroscino, A. Tampieri, Carbonated hydroxyapatite as bone substitute, Journal of European Ceramic Society 23 (2003) 2931–2937, https://doi.org/10.1016/S0955-2219(03)00304-2.

[27] Y. Sekine, T. Nankawa, T. Yamada, D. Matsumura, Y. Nemoto, M. Takeguchi, T. Sugita, I. Shimoyama, N.Kozai, S. Morooka, Carbonated nanohydroxyapatite from bone waste and its potential as a super adsorbent for removal of toxic ions, Journal of Environmental Chemical Engineering 9 (2021) 105114, https://doi.org/10.1016/j.jece.2021.105114.

[28] S. M. Naga, H. F. El-Maghraby, E. M. Mahmouda, M. S. Talaat, A. M. Ibrhim, Preparation and characterization of highly porous ceramic scaffolds based on thermally treated fish bone, Ceramics International 41 (2015) 15010–15016, http://dx.doi.org/10.1016/j.ceramint.2015.08.057.

[29] E. A. Ofudj, A. Rajendran, A. I. Adeogun, M. A. Idowu, S. O. Kareem, D. K. Pattanayak, Synthesis of organic derived hydroxyapatite scaffold from pig bone waste for tissue engineering applications, Advanced Powder Technology 29 (2018) 1–8, https://doi.org/10.1016/j.apt.2017.09.008.

[30] A. Niakan, S.Ramesh, P. Ganesan, C. Y. Tan, J. Purbolaksono, H. Chandran, S. Ramesh, W. D. Teng, Sintering behaviour of natural porous hydroxyapatite derived from

bovine bone, Ceramics International41(2015)3024–3029, http://dx.doi.org/10.1016/j.ceramint.2014.10.138

[31] M. Figueiredo, A. Fernando, G. Martins, J. Freitas, F. Judas, H. Figueiredo, Effect of the calcination temperature on the composition and microstructure of hydroxyapatite derived from human and animal bone, Ceramics International, 36 (2010) 2383–2393, https://doi.org/10.1016/j.ceramint.2010.07.016.

[32] P. Feng, P. Wu, C. Gao, Y. Yang, W. Guo, W. Yang, C. Shuai, A Multimaterial Scaffold With Tunable Properties: Toward Bone Tissue Repair, Advanced Science, 5 (2018) 1700817, DOI: 10.1002/advs.201700817.

[33] C. Shuaia, W. Yanga, P. Feng, S. Peng, H. Pan, Accelerated degradation of HAP/PLLA bone scaffold by PGA blending facilitates bioactivity and osteoconductivity, Bioactive Materials 6 (2021) 490–502, https://doi.org/10.1016/j.bioactmat.2020.09.001.

[34] C. Kim, J. W. Lee, J. H. Heo, C. Park, D. H. Kim, G. S. Yi, H. C. Kang, H. S. Jung, H. Shin, J. H. Lee, Natural bone-mimicking nanoporeincorporated hydroxyapatite scaffolds for enhanced bone tissue regeneration, Biomaterial Research (2022) 26:7, https://doi.org/10.1186/s40824-022-00253-x.

[35] R. Silva, J. Camilli, C. Bertran, N. Moreira, The use of hydroxyapatite and autogenous cancellous bone grafts to repair bone defects in rats, Int. Journal of Oral and Maxillofacial Surgery 34 (2005) 178–184, https://doi.org/10.1016/j.ijom.2004.06.005.

[36] C. V. M. Rodrigues, P. Serricella, A. B. R. Linhares, R. M. Guerdes, R. Borojevic, M. A. Rossi, M. E. L. Duarte, M. Farina, Characterization of a bovine collagen–hydroxyapatite

composite scaffold for bone tissue engineering, Biomaterials 24 (2003) 4987–4997, https://doi.org/10.1016/S0142-9612(03)00410-1.

[37] H. Yoshikawa, A. Myoui, Bone tissue engineering with porous hydroxyapatite ceramics, Journal of Artificial Organs, 8 (2005) 131–136, DOI 10.1007/s10047-005-0292-1.

[38] S. V. Patwardhan, Biomimetic and bioinspired silica: recent developments and applications, 27 (2011) 7567-7582, https://doi.org/10.1039/c0cc05648k.

[39] S. Heinemann, C. Heinemann, M. Jager, J. Neunzehn, H. P. Wiesmann, T. Hanke, Effect of Silica and Hydroxyapatite Mineralization on the Mechanical Properties and the Biocompatibility of Nanocomposite Collagen Scaffolds, Applied materials and Interface, 3 (2011) 4323-433, dx.doi.org/10.1021/am200993q.

[40] A. I. Villacampa, J. M. G. Ruiz, Synthesis of a new hydroxyapatite-silica composite material, Journal of Crystal Growth 211 (2000) 111-115, http://dx.doi.org/10.1016/S0022-0248(99)00793-9.

[41] M. K. Yadav, V. Pandey, Jyoti, A. Kumar, K. Mohanta, V. K. Singh, Mechanical and biological behaviour of porous Ti–SiO2 scaffold for tissue engineering application, Ceramics International 47 (2021) 22191–22200, https://doi.org/10.1016/j.ceramint.2021.04.242.

[42] X. Zhao, J. You, Y. Xie, H. Cao, X. Liu, Nanoporous SiO2/TiO2 composite coating for orthopedic application, Mater. Lett. 152 (2015) 53–56, https://doi.org/ 10.1016/j.matlet.2015.03.067.

[43] H. Haugen, J. Will, A. Kohler, U. Hopfner, J. Aigner, E. Wintermantel, Ceramic TiO2-foams: characterisation of a potential scaffold, Journal of the European Ceramic Society 24 (2004) 661–668, doi:10.1016/S0955-2219(03)00255-3.

[44] T. Kokubo, H. Takadama, How useful is SBF in predicting in vivo bone bioactivity, Biomaterials. 27(15) (2006) 2907–2915. DOI:10.1016/j.biomaterials.2006.01.017.

[45] J. Olsen, J. Heinemeier, P. Bennike, C. Krause, K. M. Hornstrup, H. Thrane, Characterization and blind testing of radiocarbon dating of cremated bone, Journal of Archaeological Science, 35 (2008) 791–800, https://doi.org/10.1016/j.jas.2007.06.011.

[46] B. Bogdan, I. Markovska, Y. Hristov, D. Georgiev, Light-weight materials obtained by utilization of agricultural waste, World Acad. Sci. Eng. Technol. 64 (2012) 725–728.

[47] S. F. Ou, S. Y. Chiou, K. L. Ou, Phase transformation on hydroxyapatite decomposition, Ceramics International, 39 (2013) 3809–3816, dx.doi.org/10.1016/j.ceramint.2012.10.221

[48] M. Sayer, A. D. Stratilatov, J. Reid, L. Calderin, M. J. Stott, X. Yina, M. Mackenzie, T. J. N. Smith, J. A. Hendry, S. D. Langstaff, Structure and composition of silicon-stabilized tricalcium phosphate, Biomaterials, 24 (2003) 396-382, https://doi.org/10.1016/S0142-9612(02)00327-7.

[49] J. W. Reid, A. Pietak, M. Sayer, D. Dunfield,T. J. N. Smith, Phase formation and evolution in the silicon substituted tricalcium phosphate/apatite system, Biomaterials 26 (2005), 2887-2897, https://doi.org/10.1016/j.biomaterials.2004.09.005.

[50] A. J. Ruys, Silicon-doped hydroxyapatite, Journal of Australian ceramic society 29(1993) 71.

[51] E. Kusrini, M. Sontang, Characterization of x-ray diffraction and electron spin resonance: Effects of sintering time and temperature on bovine hydroxyapatite, Radiation Physics and Chemistry, 81 (2012) 118-125, https://doi.org/10.1016/j.radphyschem.2011.10.006.

[52] C. Y. Ooi, M. Hamdi, S. Ramesh, Properties of hydroxyapatite produced by annealing of bovine bone, Ceramics International 33 (2007) 1171–1177, https://doi.org/10.1016/j.ceramint.2006.04.001.

[53] N. A. M. Barakat, M. S. Khil, A. M. Omran, F. A. Sheikh, H. Y. Kim, Extraction of pure natural hydroxyapatite from the bovine bones bio waste by three different methods, Journal of Materials Processing Technology, 209 (2009) 3408-3415, dx.doi.org/10.1016/j.jmatprotec.2008.07.040.

[54] W. Khoo, F. M. Nor, H. Ardhyananta, D. Kurniawan, Preparation of natural hydroxyapatite from bovine femur bones using calcination at various temperatures, Procedia Manufacturing 2 (2015) 196 – 201, doi: 10.1016/j.promfg.2015.07.034.

[55] A. E. M. Aguilar, A. P. Fagundes, D. L. P. Macuvele, K. Cesca, L. Porto, N Padoin, C. Soares, H. G. Riella, Green synthesis of nano hydroxyapatite: morphology variation and its effect on cytotoxicity against fibroblast, Materials Letters 284 (2021) 129013, https://doi.org/10.1016/j.matlet.2020.129013.

[56] S. L. Bee, Z. A. A. Hamid, Characterization of chicken bone waste-derived hydroxyapatite and its functionality on chitosan membrane for guided bone regeneration, Composite Part B 163 (2019) 562-573, https://doi.org/10.1016/j.compositesb.2019.01.036.

[57] S. S. A. Abidi, Q. Murtaza, Synthesis and characterization of nano-hydroxyapatite powder using wet chemical precipitation reaction, Journal of Material Science and Technolgy 30 (4) (2014) 307–310, https://doi.org/10.1016/j.jmst.2013.10.011.

[58] S. M. Latifi, M. H. Fathi, M. A. Golozar, Preparation and characterisation of bioactive hydroxyapatite–silica composite nanopowders via sol–gel method for medical applications, Advances in applied ceramics 110 (2011) 8-14, https://doi.org/10.1179/174367510X12753884125325.

[59] M. Eswaran, S. Swamiappan, B. Chokkiah, R. Dhanusuraman, S. Bharathkumar, V. K. Ponnusamy, A green and economical approach to derive nanostructured hydroxyapatite from Garra mullya fish scale waste for biocompatible energy storage applications, Materials Letters 302 (2021) 13034, https://doi.org/10.1016/j.matlet.2021.130341.

[60] B. R. Sunil, M. Jagannatham, Producing hydroxyapatite from fish bones by heat treatment, Materials Letters, 185 (2016) 411-414, https://doi.org/10.1016/j.matlet.2016.09.039

[61] G. Krishnamurithy, M. R. Murali, M. Hamdi, A. A. Abbas, H. B. Raghavendran, T.Kamarul, Characterization of bovine-derived porous hydroxyapatite scaffold and its potential to support osteogenic differentiation of human bone marrow derived mesenchymal stem cells, Ceramics International, 40 (2014) 771–777, http://dx.doi.org/10.1016/j.ceramint.2013.06.067

[62] B Mondal, S. Mondal, A. Mondal, N. Mandal, Fish scale derived hydroxyapatite scaffold for bone tissue engineering, Materials Characterization, 121 (2016) 112–124, http://dx.doi.org/10.1016/j.matchar.2016.09.034

[63] J. Triyono, R. Alfiansyah, H. Sukanto, D. Ariawan, Y. Nugroho, Fabrication and characterization of porous bone scaffold of bovine hydroxyapatite-glycerin by 3D printing technology, Bioprinting, 18 (2020) e00078, https://doi.org/10.1016/j.bprint.2020.e00078

[64] F. H. Lin, C. J. Liao, K. S. Chen, J. S. Sun, C. P. Lin, Petal-like apatite formed on the surface of tricalcium phosphate ceramic after soaking in distilled water, Biomaterials 22 (2001), 2981-2992, https://doi.org/10.1016/S0142-9612(01)00044-8..